Nematic-liquid-crystal–air interface in a radial Hele-Shaw cell: Electric field effects

Tibor Tóth-Katona* and Ágnes Buka
Research Institute for Solid State Physics and Optics, Hungarian Academy of Sciences, P.O. Box 49, H-1525 Budapest, Hungary
(Received 30 May 2002; revised manuscript received 7 February 2003; published 30 April 2003)

The influence of an external electric field (applied to the nematic liquid crystal layer) on the morphology of the nematic-liquid-crystal–air interface has been studied experimentally in radial Hele-Shaw geometry. The effective viscosity μ_{eff} of the nematic has been tuned by the electric field E and by the flow. At low excess pressure p_e (where the growth of the interface is controlled mainly by the surface tension σ), the applied E has no significant influence on the morphology of the interface, but decreases its normal velocity due to the increase of μ_{eff}. At higher p_e (where the growth is not only controlled by σ, but also by the kinetic term that depends on the effective viscosity) a significant difference in the morphology has been observed as a function of E. Experiments have shown that the influence of the electric field on the pattern morphology increases with the driving force (pressure gradient).

DOI: 10.1103/PhysRevE.67.041717 PACS number(s): 61.30.−v, 47.54.+r, 47.20.Ma

I. INTRODUCTION

The Saffman-Taylor (viscous fingering) problem has been intensively studied, since it represents a relatively simple case of nonlinear interfacial pattern formation—see, e.g., Refs. [1–4].

For the interface between two close parallel plates with separation d (Hele-Shaw cell [5]) where the less viscous fluid drives radially the more viscous one, experimental results agree well with the linear stability analysis [6]. Later stages of the interface growth in the radial geometry (after breakup of the initial circle) are less understood than those of the channel flow. For isotropic fluids, the pattern continues to evolve through repeated tip splitting to form more and more fingers.

An external perturbation or an imposed anisotropy can change dramatically the Saffman-Taylor finger and can even depress the tip-splitting process. Experiments [7–12] have demonstrated the important role of the introduced *external anisotropy* (gas bubble in front of the finger, grooves, or grid engraved on the bounding plates) in viscous fingering.

Other possibility is to introduce *intrinsic anisotropy* with the use of non-Newtonian or complex fluids (usually as a more viscous fluid) where shear thinning/thickening effects, or plastic/elastic effects, result in a much richer morphological diagram than that for isotropic fluids. Despite the complexity of the governing equations, interfacial instabilities in such fluids are subject of rapidly developing research both experimentally [13–25] and theoretically or numerically [26–31]. Besides the challenging basic research issues, these studies are of pronounced technological importance.

A number of experiments has been done in systems with nematic liquid crystals as the more viscous fluid where both the shear thinning and elastic effects are combined, see e.g., Refs. [32–38]. Four basic types of morphologies have been found in these systems: tip-splitting branches, dense branching, sparse dendritic, and dense dendritic [32,35]. The tip stabilization and the apperance of the dendritic pattern has been attributed to the viscosity anisotropy at the tip [33,34]. Recently, it has been shown by numerical simulation for isotropic fluids that non-Newtonian behavior can suppress tip splitting and produce dendritic growth with side branches [27,30].

In nematic liquid crystals the director field **n** (that describes the orientation of the nematic phase) and the velocity field **v** are coupled by nonlinear nematohydrodynamic equations—see, e.g., Refs. [39,40]. However, detailed analysis based on the precise nematohydrodynamic equations which would allow quantitative comparison with experiments is not available at the present. Questions such as the interplay between viscosity and elasticity as well as the competition between the surface tension and viscosity anisotropies are still open. The motivation of this work was to contribute to the solution of these problems, specifically to study the effect of the viscosity anisotropy along the interface by applying an electric field that provides a tool for fine tuning of the viscosity between its two limiting values. Namely, using nematic liquid crystals with dielectric anisotropy $\varepsilon_a = \varepsilon_\parallel - \varepsilon_\perp > 0$ ($\varepsilon_\parallel$ and $\varepsilon_\perp$ are components of the uniaxial dielectric tensor parallel and perpendicular to **n**, respectively), and applying an appropriate external electric field E perpendicular to the plane of the cell, one can tune the effective viscosity μ_{eff} of the more viscous fluid in the shear plane with p_e and E. To our knowledge, this is a unique system in which different μ_{eff} could be assured for the same excess pressure p_e. When the shear torque [40] exerted on the director is much larger than the electric torque (high p_e and low E, elastic torques are negligible in our case), the effective viscosity $\mu_{eff} \approx \eta_1$. In the opposite case, when the electric torque is much larger than the shear torque, we have $\mu_{eff} \approx \eta_2$ (η_1 and η_2 are the corresponding Miezowitz viscosity coefficients—see, e.g., Ref. [40]). Consequently, in the experiments μ_{eff} can be tuned in the range of

$$\eta_1 \leqslant \mu_{eff} \leqslant \eta_2 . \tag{1.1}$$

Finally, one should mention that the reorientation of the director tunes the surface tension σ of the air-nematic interface too in the range of

*Corresponding author. Present address: Physics Department, Kent State University, P.O. Box 5190, Kent, OH 44242-0001.

$$\sigma_{\parallel} \leqslant \sigma \leqslant \sigma_{\perp}, \tag{1.2}$$

where $\sigma_{\parallel}$ and $\sigma_{\perp}$ are the surface free energies for the interface parallel and perpendicular to **n**, respectively. However, the change in the surface free energy from $\sigma_{\parallel}$ to $\sigma_{\perp}$ is in the range of only 20–50 % for different nematic substances [41], while the anisotropy in the viscosity is much larger: $\eta_2 \simeq 5\,\eta_1$ far below the nematic-isotropic phase transition temperature (T_{NI})—see, e.g., Refs. [42,43].

II. EXPERIMENTAL SYSTEM

In the experiments two commercial liquid-crystalline substances have been used, both having positive dielectric anisotropy and a broad temperature range of the nematic phase: ZLI-2116-100 (Merck, $\varepsilon_a = 3.7$, $T_{NI} = 95\,^{\circ}\mathrm{C}$) and RO-TN-430 (La Roche, $\varepsilon_a = 17.6$, $T_{NI} = 70\,^{\circ}\mathrm{C}$). Both substances have been doped with dichroic blue dye D16 British Drug House in order to enhance the contrast at the air-nematic interface, and to enhance the visual effects of changes in the orientation of **n**.

Two different radial Hele-Shaw cells have been used. Cell 1 was made of 3.1 mm thick glass plates. The whole inner surface of the bottom plate of dimensions (90×90) mm^2 and only one-half of the upper plate of dimensions (80×80) mm^2 have been coated with SnO_2. Such electrode geometry has allowed to apply E only on one-half of the cell and consequently, to study pattern forming processes with different μ_{eff} simultaneously. Cell 2 was made from 5.5 mm thick float-glass plates. The inner surfaces of both bottom and upper plates have been coated with a conductive layer. The dimension of the squared bottom plate was (160×160) mm^2, while the circular upper plate had a diameter of 140 mm. In most of the experiments the plates were separated by $d = 100$ μm thick spacers. Air was injected at constant p_e through the hole of 1 mm in diameter in the center of one of the plates. The inner surfaces of the bounding glass plates had no special treatment except a careful cleaning. This cleaning procedure, however, gave a homeotropic anchoring (i.e., director perpendicular to the plates) when $p_e = 0$. The director orientation has been detected by means of birefringence.

The pressure of the filtered air has been regulated by ported precision regulator (model: Norgren 11-818-100) with an accuracy of ± 0.03 bar. A unit for pressure reduction has been also used that decreases further the pressure and enhance its stability. The path of the air has been controlled by two three-path solenoid valves. The pressure p_e has been measured by precision pressure meter (Watson&Smith) with an accuracy of ± 1 mbar. The temperature of the cell has been regulated by a hot stage with an accuracy of $\pm 1\,^{\circ}\mathrm{C}$. In all the experiments in which E has been applied we used an ac field with a frequency of 1 kHz. The growth processes have been recorded onto video tape. The recorded images were fed into a PC for digital analysis, with spatial resolution of 512×512 pixels and 256 gray scaling for each pixel. With the magnifications used in the experiments spatial resolutions of $(0.175 \times 0.123) mm^2$/pixel and $(0.241 \times 0.166) mm^2$/pixel have been determined for cell 1 and cell 2, respectively.

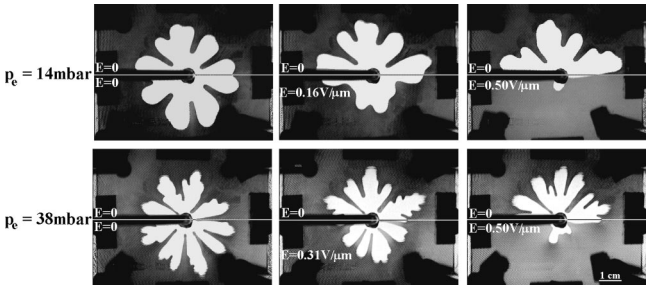

FIG. 1. Influence of the electric field in cell 1 filled with ZLI-2116-100. Two series of experiments with different p_e at $T = 32\,^{\circ}\mathrm{C}$. For each subfigure $E = 0$ in the upper half plane, while in the lower half plane $E = 0$; 0.16 V/μm; 0.50 V/μm for $p_e = 14$ mbar and $E = 0$; 0.31 V/μm; 0.50 V/μm for $p_e = 38$ mbar.

One of the most critical issues in the viscous fingering experiments is the plate deformation [13,15,22]. Following the work of Ref. [13], we have estimated the deformation of the glass plates occuring under pressure. Even under the most pessimistic assumptions (high pressure, large lateral dimensions, 3.1-mm-thin plates), it appears that the plate deformation did not exceed 6% of the cell gap. Based on an independent test performed in Ref. [15], we assume that this does not effect the pattern morphology significantly.

III. RESULTS

A. Electric field effects

Simultaneous observation of the pattern evolution with and without E has been performed using cell 1, where only one-half of the cell has been exposed to E. Consequently, in these experiments for given values of p_e and E one has different μ_{eff} in the two halves of the cell. Fig. 1 shows two series of such experiments with $p_e = 14$ mbar and $p_e = 38$ mbar and with different E ranging from 0 to 0.5 V/μm. The cell was filled with ZLI-2116-100 and the temperature was $T = 32\,^{\circ}\mathrm{C}$. As it can be seen, the motion of the interface is slower in the half plane where E is applied.

In Fig. 2(a), the ratio A_2/A (A is the complete area of the pattern and A_2 is the pattern's area in the half plane with $E \neq 0$) has been plotted as a function of E for different values of p_e ranging from 5 mbar to 38 mbar. Ideally, for $E = 0$ one should have $A_2/A = 0.5$. Figure 2(a) shows that A_2/A is slightly above 0.5 for all values of p_e in case of $E = 0$. This is presumably caused by the differences in wetting properties (one-half of the upper plate is coated with SnO_2 while the other half is not). For low p_e, the ratio A_2/A decreases and saturates to the value of about 0.1 already at low values of E. Naturally, the higher p_e requires higher E for such saturation.

One can construct a "threshold curve" $E_{th}(p_e)$ that divides the so called basic state from the state perturbed by E in the (p_e, E) plane. In the basic state the influence of E on the interface motion is not detectable (i.e., $A_2/A = 0.5$ or slightly larger because the above described differences in the wetting properties), contrary to the perturbed state where $A_2/A < 0.5$. Such a threshold curve is presented in Fig. 2(b) and it appears to be linear as a function of p_e.

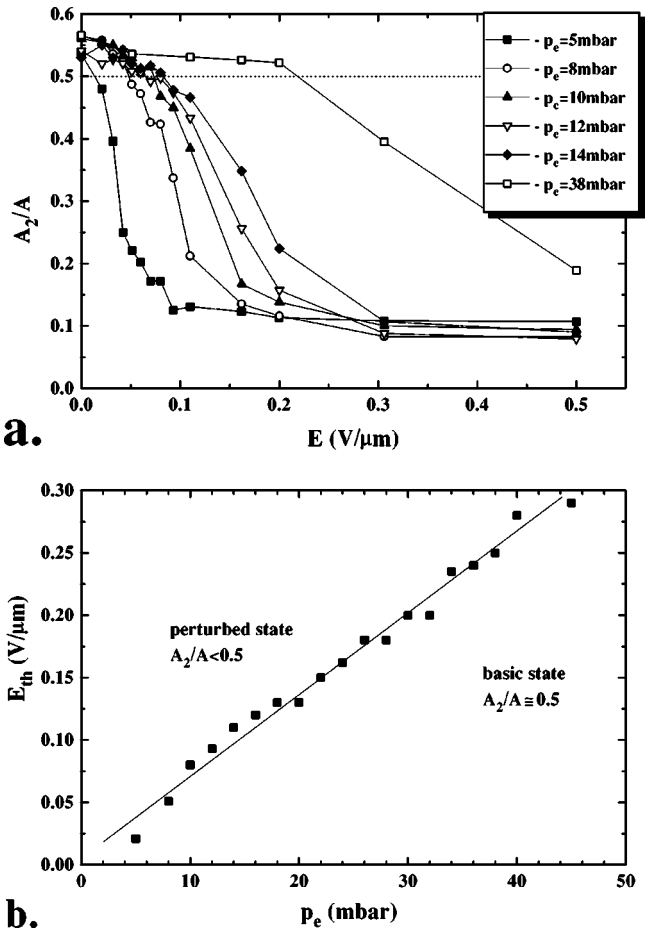

FIG. 2. (a) Ratio of A_2/A versus E for different p_e. (b) The ''threshold curve'' dividing the basic state from the state perturbed by E.

B. Temperature effects

Similar experiments to that presented in Fig. 1 have been performed at different temperatures ranging from $T=30\,^{\circ}\mathrm{C}$ to $T=97\,^{\circ}\mathrm{C}$. The latter temperature is just above the nematic-isotropic phase transition $T_{NI}=95°$. Figure 3 shows the time evolution of the interface for $p_e=12$ mbar at three different temperatures: $T=31\,^{\circ}\mathrm{C}$, $T=92\,^{\circ}\mathrm{C}$ (both in the nematic phase), and $T=97\,^{\circ}\mathrm{C}$ (in the isotropic phase). The interface motion becomes faster as the temperature increases. This is in accordance with the temperature dependences of the viscosity coefficients—see, e.g., Refs. [42,43].

The ratio of A_2/A is also indicated in Fig. 3. For $E=0$ on both half-planes of the cell, the value of A_2/A has been found for each T to be slightly above 0.5 [see Figs. 3(a–c)] due to the differences in the wetting properties on the two parts of the cell described in the preceding section. For $E=0.5$ V/μm on the bottom half plane A_2/A has been found to be much smaller than 0.5 in the nematic phase [see Figs. 3(d) and 3(e)] due to the much higher μ_{eff} in the bottom half plane from that in the upper one. We found a jump in the value of A_2/A at T_{NI} which shows that the effect is due to a liquid-crystalline property, presumably the anisotropy of μ. In the isotropic phase, A_2/A is slightly below 0.5 [see Fig. 3(f)]. The small difference in A_2/A shown in Figs. 3(c) and 3(f) is presumably the consequence of a dielectric effect when the isotropic liquid with ε is replaced by air with ε_0.

In the nematic phase itself the A_2/A also increases slightly with the temperature [cf. Figs. 3(d) and 3(e)]. This can be understood by the temperature dependence of the Miezowitz viscosity coefficients η_1 and η_2 in most of the nematics, where both η_1 and η_2 decrease with the decrease of temperature but with different slopes: η_2 decreases faster with decreasing temperature than η_1 (see Refs. [42,43]). Moreover, just below T_{NI}, the slope of η_1 changes sign—it increases with temperature approaching the viscosity of the

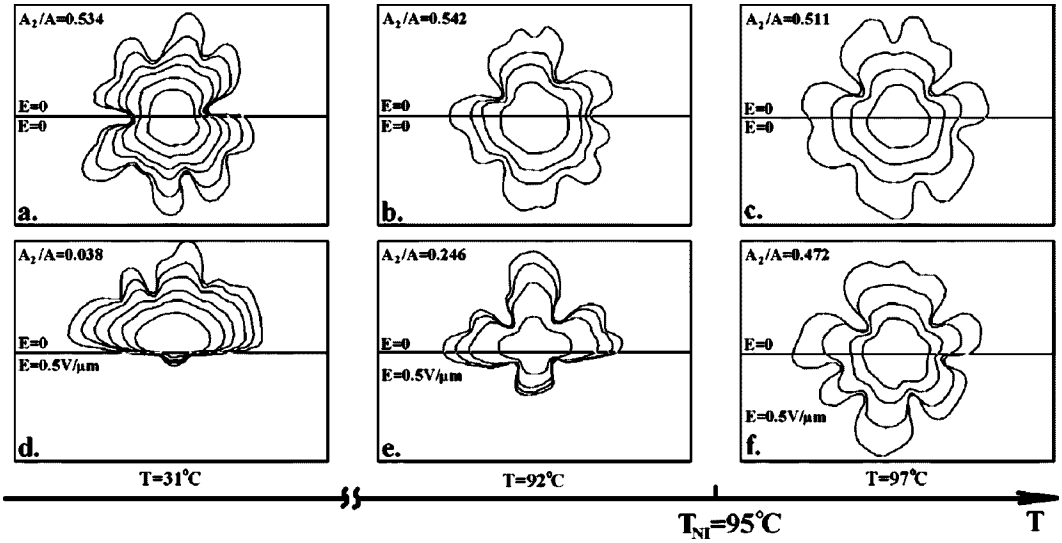

FIG. 3. Influence of the temperature and that of E on the interface motion for $p_e=12$ mbar at three different temperatures $T=31\,^{\circ}\mathrm{C}$, $T=92\,^{\circ}\mathrm{C}$, and $T=97\,^{\circ}\mathrm{C}$. The ratio A_2/A as well as values of E in both half planes are indicated in each part. Each part consists of contours of the interface taken at subsequent times on top of each other: (a) $t=1.3$ s, 2.5 s, 3.9 s, 4.9 s, 6.3 s, 7.4 s; (b) $t=0.3$ s, 0.6 s, 0.8 s, 1.1 s; (c) $t=0.3$ s, 0.6 s, 1.0 s, 1.5 s; (d) $t=2.8$ s, 4.2 s, 5.3 s, 6.6 s, 7.6 s, 8.6 s; (e) $t=0.3$ s, 0.7 s, 0.9 s, 1.0 s; (f) $t=0.4$ s, 0.7 s, 1.1 s, 1.5 s.

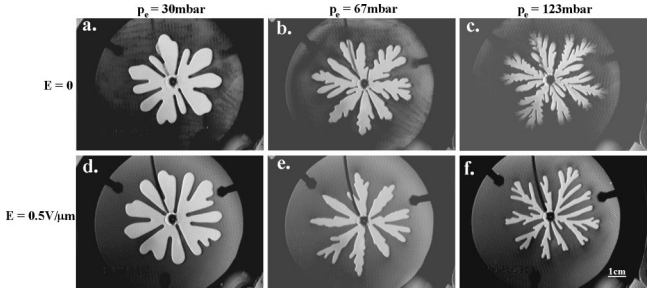

FIG. 4. Influence of the electric field on the pattern formation in the $d=100$ μm thick cell 2 filled with RO-TN-430. E and p_e are indicated in the figure. The elapsed times of the growth are (a) 5.5 s, (b) 1.5 s, (c) 0.4 s, (d) 26.5 s, (e) 5.1 s, and (f) 1.2 s.

isotropic phase μ_{iso} that is slightly larger than η_1 below T_{NI}. In the nematic phase with $E\neq 0$ [as in Figs. 3(d) and 3(e)], one can assume $\mu_{eff}\approx\eta_2$ in bottom half plane of the cell, while in the upper half plane $\mu_{eff}\approx\eta_1$. This assumption leads to the result observed in the experiments: A_2/A increases slightly with the temperature, the increment becomes more pronounced as T_{NI} is approached, and one has a jump in A_2/A at T_{NI}. Moreover, with the above described assumptions one can explain that the interface motion is slower in the isotropic phase just above T_{NI} [Fig. 3(c)] than that in the nematic phase just below T_{NI} [Fig. 3(b)]. Namely, in the first case one has $\mu_{eff}\approx\eta_1$ and in the latter case $\mu_{eff}=\mu_{iso}$, while $\eta_1<\mu_{iso}$.

C. Circular cell geometry

The strong influence of E on the interface motion has been demonstrated in the cell 1 that allowed observation of the pattern evolving with E on and off simultaneously in a single experimental run. However, this cell geometry has some disadvantages: besides the different wetting properties on the two half planes, E is inhomogeneous near the line that divides the two half planes, moreover, this line may represent an external anisotropy. For these reasons, cell 2 has been used for direct comparison of the patterns appearing with E off and E on.

Two series of experiments (with $E=0$ and $E=0.5$ V/μm) have been carried out at room temperature $T=23\,^{\circ}$C for p_e ranging from 30 mbar to 123 mbar. Figure 4 shows snapshots of the patterns for different p_e and for both $E=0$ and $E=0.5$ V/μm in the $d=100$ μm thick cell filled with RO-TN-430. Obviously, the difference between the morphologies with E off and E on becomes more pronounced for higher p_e. At low p_e, patterns observed with E off and E on are similar: in both cases the interface evolves through repeated tip splitting [cf. Figs. 4(a) and 4(d)]. In the intermediate range of p_e the qualitative difference between the patterns with E on and off is obvious—the pattern with E on is rather side branching [dendritic, Fig. 4(e)], contrary to E off where it is more tip splitting [Fig. 4(b)]. For large p_e, however, tip splitting has been observed for both E off and on, but in the latter case the pattern was found to be more sparse [cf. Figs. 4(c) and 4(f)]. The velocity of the interface is much lower with E on than with E off; however, the relative difference in the velocities decreases with the increase of p_e (compare elapsed times of the growth indicated in the figure caption of Fig. 4).

At low p_e with E off [Fig. 4(a)] the shear torque is still large enough to produce flow alignment, i.e., one clearly observes a director reorientation from the initial homeotropic to radial alignment when p_e is applied so that, $\mu_{eff}\approx\eta_1$ and (if one assumes that the flow alignment persists at the interface) $\sigma\approx\sigma_{\perp}$. Naturally, the same applies for higher p_e too [Figs. 4(b) and 4(c)]. With E off even for the smallest $p_e=5$ mbar (when the air bubble starts to grow) a reorientation of the director has been clearly detected by the means of birefringence. Note that in all experiments presented here a dichroic dye has been used as a dopant to enhance the contrast at the interface, and all the images were recorded with a single polarizer. Test measurements with two (crossed) polarizers have been also performed and led to the same conclusion: with E off for $p_e\geqslant 5$ mbar a reorientation front has been observed in the form of rapidly advancing circular reorientation wave (however, with crossed polarizers the recorded images appeared more complicated due to a thin liquid-crystalline layer left behind the air-nematic interface due to the wetting reducing significantly the contrast). The observation of the reorientation wave at $p_e=5$ mbar (with E off) is in accordance with previous studies that have also shown that the initial alignment of the nematic director does not influence the patterns (see, e.g., Ref. [38]) and therefore, the elastic torque is much smaller than the shear torque in any of the experiments presented here.

With E on, however, at low p_e [Fig. 4(d)] the electric torque turned out to be larger than the shear one—homeotropic orientation has been clearly detected even close to the interface—so that $\mu_{eff}\approx\eta_2$ and $\sigma\approx\sigma_{\parallel}$. Consequently, at low p_e by applying strong enough E, μ_{eff} (that influences the time scale of the growth) increases by a factor of about 3–4 compared to the case $E=0$ (for estimation of the viscosities with E off and on see the following section). This explains why the pattern shown in Fig. 4(d) grows much slower than that presented in Fig. 4(a). Surface tension—which at low p_e mainly controls the growth of the interface—differs also with E off and on, but this difference should not be larger than tipically 30% according to Refs. [42,43]. Such a relatively small difference between $\sigma_{\perp}$ and $\sigma_{\parallel}$ could explain the similarity of the morphologies shown in Figs. 4(a) and 4(d).

At intermediate p_e [Fig. 4(e)], however, the shear torque becomes comparable with that of the electric. The director field has been found experimentally (again by means of birefringence) to be inhomogeneous. Just in front of the tips a deviation from the homeotropic alignment has been detected, while in other parts of the cell (at the lateral sides of the tips and far from the interface) the orientation remained homeotropic. In this case the balance of the electric and shear torques presumably results in a director field which makes an angle larger than the Leslie angle Θ_0 with the velocity. This means that both the viscosity and the surface tension become anisotropic in the shear plane near the tip that leads to stabilization of the tip and to a transition from tip splitting to side branching as seen in the experiments [cf. Figs. 4(b) and

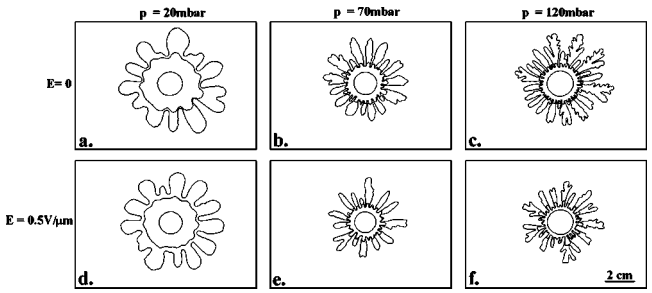

FIG. 5. Growth from an initial circular bubble in the $d=100$ μm thick cell 2 filled with RO-TN-430. E and p_e are indicated in the figure. Each part consists of contours of the interface taken at subsequent times on top of each other: (a) $t=0$, 6.9 s, 13.5 s; (b) $t=0$, 0.3 s, 0.7 s; (c) $t=0$, 0.1 s, 0.3 s; (d) $t=0$, 20.5 s, 49.7 s; (e) $t=0$, 1.0 s, 2.5 s; (f) $t=0$, 0.2 s, 0.6 s.

4(e)]. On the other hand, deviations from the homeotropic alignment in the intermediate p_e range lead to the decrease of the viscosity in the shear plane compared to that in the low p_e range. This explains the lowering of the relative difference in the interface velocities for intermediate p_e [Figs. 4(b) and 4(e)] compared to that for low p_e [Figs. 4(a) and 4(d)].

For large p_e [Fig. 4(f)], deviation from the homeotropic alignment in front of the tip is even more distinguishable and the tip splitting reappears. However, far from the interface and at the lateral sides of the tip the orientation remains nearly homeotropic with larger effective viscosity than that in front of the tip, producing more ''elongated'' tips compared to those with E off [Fig. 4(c)] and resulting a more sparse pattern. The observed reappearance of the tip splitting growth mode is in accordance with other experiments in liquid crystals, where dendritic growth has been detected only in a certain range of p_e [34,38]. In Ref. [34] it has been shown that for the tip stabilization (side branching, dendritic growth), a critical value of the viscosity ratio μ_t/μ_r (μ_t and μ_r are the viscosities in the tangential and in the radial direction to the tip) is needed. This is the reason why stable dendritic tips are observable over a certain range of p_e only. Namely, at high p_e (high Er) the probability of defect creation (spatial inhomogeneities in **n**) increases, and shear instabilities can also occur. Both of these phenomena tend to destroy the laminar flow (and the shear alignment) and with that, the viscosity anisotropy (maintaining the stable dendritic growth) tends to diminish resulting in the reappearance of the tip splitting growth mode.

Note the striking similarities between our Fig. 4 and experimental results obtained in aqueous glycerol and hydroxypropyl methyl cellulose (HPMC) solutions where an increase of isopropyl alcohol content led to a decrease in σ as well as an increase in η [21,22], i.e., to a similar situation that is achieved by application of E in our experiments. For the Newtonian glycerol solutions the increase of the isopropyl alcohol content caused finger narrowing and an increase of the number of fingers. In contrast, for the shear-thinning HPMC solutions, a morphological transition has been reported [21] with the increase of the alcohol content. Without isopropyl alcohol a highly branched pattern has been detected [similar to that shown in Fig. 4(c)], while with an increase of the alcohol content the branching growth has been suppressed resulting in less space filling pattern [similar to our Fig. 4(f)].

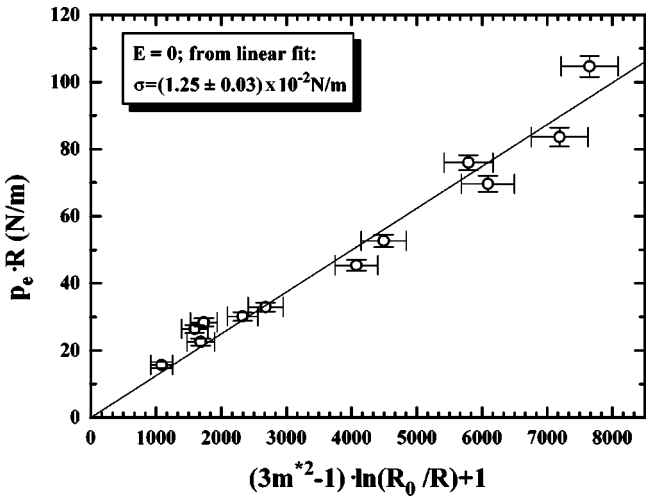

FIG. 6. Rough estimation of the surface tension from the linear stability analysis for RO-TN-430.

D. Destabilization of the circular bubble

Inhomogeneities on the bounding glass plate at the hole used as inlet for the air may influence the number of fingers formed in the fingering process. Therefore, one can obtain much more precise experimental results starting the growth from an initial air bubble kept in equilibrium at a finite radius. Figure 5 shows contours of patterns grown in similar condition as those in Fig. 4, but starting the growth from an initial air bubble. Qualitatively, the main characteristics of the patterns in Fig. 5 are similar to those presented in Fig. 4: the difference between the morphologies with E off and on becomes more pronounced by the increase of p_e; at low p_e the patterns with E off and on are quite similar [cf. Figs. 5(a) and 5(d)]; the velocity of the interface is much lower with E off than with E on, but the relative difference in the velocities decreases with the increase of p_e (compare the times of growth indicated in the figure caption of Fig. 5). The only exception is that the tip stabilization in the intermediate range of p_e is not so obvious in Fig. 5(e) as in Fig. 4(e).

One can make a rough estimation of σ by observing the first destabilization of the circular interface. Namely, neglecting the kinetic term (acceptable approximation at low p_e only), linear stability analysis of the circular interface leads to the expression [33]

$$m^*=\left[\frac{1}{3}\left(\frac{\left(\frac{p_eR}{\sigma}-1\right)}{\ln(R_0/R)}+1\right)\right]^{1/2} \tag{3.1}$$

for the fastest growing mode m^*. Here R is the radius of the circular interface and R_0 is the cell radius. Consequently, m^* is independent of the viscosity and depends only on the ratio of p_e/σ. Experiments at low p_e (where the kinetic term can

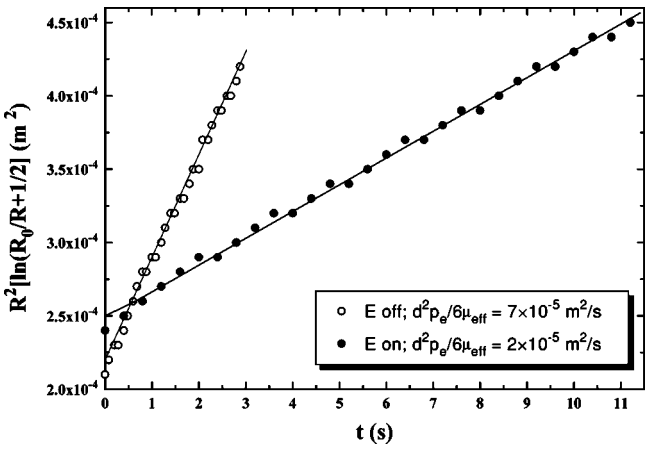

FIG. 7. Estimation of effective viscosities for RO-TN-430 with E off (open circles) and E on (filled circles).

be omitted) in the isotropic phase of liquid crystal 8CB gave results in good agreement with Eq. (3.1) [33].

Figure 6 shows a graph for such estimation of the surface tension with E off (which would correspond to $\sigma_\perp$ assuming flow alignment in the sample). From the slope of the fitted straight line a value of $\sigma_\perp=(1.25\pm0.03)\times10^{-2}$ N m has been obtained, which is a slightly smaller value (by about 30–50 %) from those obtained for several other nematic-liquid-crystal–air interfaces [41]. As one can see in Fig. 5 (second contours in time), the number of perturbations for the first destabilization of the circular interface does not differ significantly for E off and E on for a given p_e. This indicates that the anisotropy of the surface tension is smaller than that detectable with such a rough estimation method.

From the growth of the circular interface one can estimate the value of the effective viscosity. Namely, the normal velocity with which a circular interface propagates is given by [34]

$$v_n=\frac{d^2}{12\mu}\left[p_e-\sigma\left(\frac{1}{R}-\frac{1}{R_0}\right)\right]\frac{1}{R\ln(R_0/R)}. \tag{3.2}$$

If one neglects the term $\sigma[(1/R)-(1/R_0)]$ (which is in our case by orders of magnitude smaller than p_e), one can obtain from Eq. (3.2)

$$R^2\left[\ln\left(\frac{R_0}{R}\right)+\frac{1}{2}\right]=\frac{d^2p_e}{6\mu}t, \tag{3.3}$$

i.e., by plotting the left hand side of Eq. (3.3) as a function of t (Fig. 7), the slope gives the value of $d^2p_e/6\mu$ from which the viscosity can be calculated. From the slopes in Fig. 7 values of $\eta_1\approx\mu_{eff}=0.045$ Pa s (with $d=100$ μm and $p_e=1900$ Pa) and $\eta_2\approx\mu_{eff}=0.167$ Pa s (with $d=100$ μm and $p_e=2000$ Pa) have been obtained with E off and on, respectively. These values are in the range of the viscosities measured for other nematic liquid crystals [42,43], and reflect the high anisotropy in the viscosity (common to nematic liquid crystals), which presumably plays a decisive role in achieving morphological transitions presented above.

To our knowledge for the materials used in present experiments the viscosities and the elastic constants K_i are not available (in fact, our experiments gave only an admittedly crude estimate of the corresponding Miesowitz viscosity coefficients). Moreover, an applied electric field gives an extra torque counteracting the flow alignment of the director. All these facts prevent us to give a precise quantitative calculation of the corresponding Ericksen number $Er=\mu_{eff}v_nd/K_i$ and the torques Γ_i acting. However, taking the known parameters for our substance and substituting the missing ones with data for a commonly used liquid crystal MBBA, we can make an estimation of Er and the torques.

First, we can roughly estimate the velocity v_{reor} of the front at which the complete flow alignment should occur (for details see, e.g., Ref. [40]). These calculations give $v_{reor}\sim4\times10^{-5}$ m/s leading to an $Er\approx100$ (taking the known Leslie viscosity coefficients α_i and the relevant K_3 elastic coefficient for MBBA—see, e.g., Ref. [45]). On the other hand, our measurements made at the lowest $p_e=5$ mbar give $v_n\approx40\times10^{-5}$ m/s and $Er\approx1000$, i.e., both the v_n and Er larger by about an order of magnitude than the values where the complete shear alignment should take place. This means that already at the smallest p_e applied we are well above the reorientation threshold as experimentally observed.

Second, a rough estimation of the torques acting on the unit of volume in our experiments leads us to the following results: (i) elastic torque $\Gamma_{el}\approx0.01$ N/m^2, with $K_3=7\times10^{-12}$ N measured for MBBA; (ii) electric torque $\Gamma_E=\mathbf{n}\times[\varepsilon_a(\mathbf{n}\cdot\mathbf{E})\mathbf{E}/4\pi]\approx3$ N/m^2 with $E=0.5$ V/μm applied in our experiments; (iii) shear torque in case shown in Fig. 5(d) is $\Gamma_s=\alpha_2v_n/d\approx0.3$ N/m^2, while for that shown in Fig. 5(e) $\Gamma_s\approx4$ N/m^2 ($\alpha_2=-0.0775$ Pa s taken again for MBBA).

As one can see again, Γ_{el} is negligible compared to Γ_s and Γ_E. Note also that at small p_e [Fig. 5(d)] $\Gamma_E\gg\Gamma_s$ and consequently, the homeotropic orientation should persist as observed in the experiments. At $p_e=70$ mbar, however, $\Gamma_E\sim\Gamma_s$ and a competition occurs between these two torques: on the spatial spots in Fig. 5(e) where v_n is relatively large (in front of the tips) Γ_s prevails and the director reorients. This explains the experimental observation of the nonhomogeneus director field at this (and larger) p_e.

IV. CONCLUDING REMARKS

We have shown experimentally that a morphological transition can be induced at the air—nematic-liquid-crystal interface by applying an appropriate electric field E. Namely, a strong enough E (for a given p_e) reorients the director field which tunes the viscosity, the surface tension, and the anisotropy of these quantities in the shear plane.

We have also estimated material parameters σ and μ_{eff} (quantities which are not easy to determine experimentally), and we found values that are in a reasonable agreement with the values measured for other nematic liquid crystals.

The experimental observation that the morphological transition occurs at higher p_e, and since the anisotropy in the viscosity seems to be much larger than that in the surface tension, indicates that the high anisotropy in the viscosity

plays a decisive role in achieving the presented morphological transitions.

Finally, one should mention that the method described here could be useful in studying the side branching process by application of a modulated E [44], or with the help of the bounding glass plates having electrodes with various special geometries.

ACKNOWLEDGMENTS

The authors wish to thank Professor L. Kramer, Professor A. Hernández-Machado, and R. Folch for fruitful discussions. This work was financially supported by the National Scientific Research Foundation Grant Nos. F022771 and OTKA T031808.

[1] G. Homsy, Annu. Rev. Fluid Mech. **19**, 271 (1987).
[2] D. Bensimon, L. Kadanoff, S. Liang, B. Shraiman, and C. Tang, Rev. Mod. Phys. **58**, 977 (1986).
[3] P. Saffman, IMA J. Appl. Math. **46**, 137 (1991).
[4] K. McCloud and J. Maher, Phys. Rep. **260**, 139 (1995).
[5] H. Hele-Shaw, Nature (London) **58**, 34 (1898).
[6] L. Paterson, J. Fluid Mech. **113**, 513 (1981).
[7] Y. Couder, O. Cardoso, D. Dupuy, P. Tavernier, and W. Thom, Europhys. Lett. **2**, 437 (1986).
[8] Y. Couder, N. Gerard, and M. Rabaud, Phys. Rev. A **34**, 5175 (1986).
[9] M. Matsushita and H. Yamada, J. Cryst. Growth **99**, 161 (1990).
[10] E. Ben-Jacob, R. Godbey, N.D. Goldenfeld, J. Koplik, H. Levine, T. Müller, and L.M. Sander, Phys. Rev. Lett. **55**, 1315 (1985).
[11] E. Ben-Jacob and P. Garik, Nature (London) **343**, 523 (1990).
[12] V. Horváth, T. Vicsek, and J. Kertész, Phys. Rev. A **35**, 2353 (1987).
[13] E. Lemaire, P. Levitz, G. Daccord, and H. van Damme, Phys. Rev. Lett. **67**, 2009 (1991).
[14] H. Zhao and J.V. Maher, Phys. Rev. A **45**, R8328 (1992).
[15] H. Zhao and J.V. Maher, Phys. Rev. E **47**, 4278 (1993).
[16] S.S. Park, and D.J. Durian, Phys. Rev. Lett. **72**, 3347 (1994).
[17] K. Makino, M. Kawaguchi, K. Aoyama, and T. Kato, Phys. Fluids **7**, 455 (1995).
[18] D. Bonn, H. Kellay, M. Ben Amar, and J. Meunier, Phys. Rev. Lett. **75**, 2132 (1995).
[19] D. Bonn, H. Kellay, M. Bräunlich, M. Ben Amar, and J. Meunier, Physica A **220**, 60 (1995).
[20] M. Kawaguchi, K. Makino, and T. Kato, Physica A **246**, 385 (1997).
[21] M. Kawaguchi, K. Makino, and T. Kato, Physica D **105**, 121 (1997).
[22] M. Kawaguchi, A. Shibata, K. Shimomoto, and T. Kato, Phys. Rev. E **58**, 785 (1998).
[23] O. Greffier, A. Al kahwaji, J. Rouch, and H. Kellay, Phys. Rev. Lett. **81**, 3860 (1998).
[24] A. Lindner, D. Bonn, and J. Meunier, Phys. Fluids **12**, 256 (2000).
[25] M. Kawaguchi, Y. Hibino, and T. Kato, Phys. Rev. E **64**, 051806 (2001).
[26] L. Kondic, P. Palffy-Muhoray, and M.J. Shelley, Phys. Rev. E **54**, R4536 (1996).
[27] L. Kondic, M.J. Shelley, and P. Palffy-Muhoray, Phys. Rev. Lett. **80**, 1433 (1998).
[28] E.C. Poiré and M. Ben Amar, Phys. Rev. Lett. **81**, 2048 (1998).
[29] M. Ben Amar and E.C. Poiré, Phys. Fluids **11**, 1757 (1999).
[30] R. Folch, J. Casademunt, and A. Hernández-Machado, Phys. Rev. E **61**, 6632 (2000).
[31] P. Fast, L. Kondic, M.J. Shelley, and P. Palffy-Muhoray, Phys. Fluids **13**, 1191 (2001).
[32] Á. Buka, J. Kertész, and T. Vicsek, Nature (London) **323**, 424 (1986).
[33] Á. Buka and P. Palffy-Muhoray, Phys. Rev. A **36**, 1527 (1987).
[34] Á. Buka, P. Palffy-Muhoray, and Z. Rácz, Phys. Rev. A **36**, 3984 (1987).
[35] Á. Buka and P. Palffy-Muhoray, J. Phys. (France) **49**, 1319 (1988).
[36] L. Lam, H. Morris, R. Shao, S. Yang, Z. Liang, S. Zheng, and H. Liu, Liq. Cryst. **5**, 1813 (1989).
[37] A. Sonin, Riv. Nuovo Cimento **14**, 1 (1991).
[38] Á. Buka, in *Pattern Formation in Liquid Crystals*, edited by Á. Buka and L. Kramer (Springer, New York, 1996), p. 291.
[39] H. Pleiner and H. Brand, in *Pattern Formation in Liquid Crystals*, edited by Á. Buka and L. Kramer (Springer, New York, 1996), p. 15.
[40] E. Dubois-Violette and P. Mannewille, in *Pattern Formation in Liquid Crystals*, edited by Á. Buka and L. Kramer (Springer, New York, 1996), p. 91.
[41] V. Tsvetkov, O. Tsvetkov, and V. Balandin, Mol. Cryst. Liq. Cryst. **329**, 305 (1999).
[42] H. Kelker and R. Hatz, in *Handbook of Liquid Crystals* (Verlag Chemie, Weinheim, 1980).
[43] C. Gähwiller, Mol. Cryst. Liq. Cryst. **20**, 301 (1973).
[44] R. Folch, T. Tóth-Katona, Á. Buka, J. Casademunt, and A. Hernández-Machado, Phys. Rev. E **64**, 056225 (2001).
[45] P.G. de Gennes and J. Prost, *The Physics of Liquid Crystals* (Clarendon Press, Oxford, 1993).